Talanta 277 (2024) 126382

Contents lists available at ScienceDirect

Talanta

journal homepage: www.elsevier.com/locate/talanta

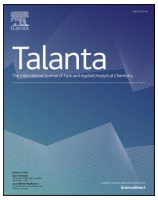

A dual-response ratiometric fluorescent sensor for oxytetracycline determination in milk and mutton samples

Mengjia Guo [a], Ming Bi [b], Fangmei Zhang [c], Xiwen Ye [a], Pinyi Ma [a,**], Dejiang Gao [a,***], Daqian Song [a,*]

[a] College of Chemistry, Jilin Province Research Center for Engineering and Technology of Spectral Analytical Instruments, Jilin University, Qianjin Street 2699, Changchun, 130012, China
[b] Hospital of Stomatology, Jilin University, Qinghua Road 1500, Changchun, 130012, China
[c] XNA Platform, Institute of Pharmaceutical Sciences, School of Pharmaceutical Sciences, Zhengzhou University, Zhengzhou, 450001, China

ARTICLE INFO

Keywords:
Oxytetracycline
Ratiometric fluorescence sensor
Molybdenum sulfide quantum dots
Europium ions
Visual analysis

ABSTRACT

Owing to the adverse effects of oxytetracycline (OTC) residues on human health, it is of great importance to construct a rapid and effective strategy for OTC detection. Herein, we developed a dual-response fluorescence sensing platform based on molybdenum sulfide quantum dots (MoS_2 QDs) and europium ions (Eu^{3+}) for ratiometric detection of OTC. The MoS_2 QDs, synthesized through an uncomplicated one-step hydrothermal approach, upon OTC integration into the MoS_2 QDs/Eu^{3+} sensing system, exhibit a significant quenching of blue fluorescence due to the inner filter effect (IFE), simultaneously enhancing the distinct red emission of Eu^{3+} at 624 nm, a phenomenon attributed to the antenna effect (AE). This sensor demonstrates exceptional selectivity and sensitivity towards OTC, characterized by a linear detection range of 0.2–10 μM and a notably low detection limit of 2.21 nM. Furthermore, we achieved a visual semi-quantitative assessment of OTC through the discernible fluorescence color transition from blue to red under a 365 nm ultraviolet lamp. The practical applicability of this sensor was validated through the successful detection of OTC in milk and mutton samples, underscoring its potential as a robust tool for OTC monitoring in foodstuffs to safeguard food safety.

1. Introduction

Oxytetracycline (OTC), a member of the tetracycline family, is a broad-spectrum antibiotic extensively employed both as a therapeutic agent against bacterial infections and as a growth-promoting feed additive in the fields of animal husbandry and aquaculture, attributed to its superior antibacterial efficacy and growth enhancement capabilities [1–3]. Despite its beneficial applications, the misuse or overuse of OTC, whether through acute overdose or prolonged low-dosage administration, can result in the persistence of antibiotic residues in animal-derived products such as milk, meat, and eggs [4]. These residues pose significant health risks, potentially inducing allergic reactions, liver damage, and contributing to the alarming escalation of antibiotic resistance among pathogens [5–7]. In response to these concerns, numerous countries have established maximum residue limits (MRLs) for OTC in food products to safeguard consumer health. Specifically, the World Health Organization (WHO) has designated an MRL for OTC in milk at 0.1 μg/mL (0.22 μM) [8], underscoring the imperative for a straightforward, expedient, and accurate methodology for the quantification of OTC residues in foodstuffs to ensure public health and food safety.

A multitude of analytical techniques for OTC monitoring has emerged, each with its specific advantages. Traditional methods, such as high-performance liquid chromatography [9], liquid chromatography-mass spectrometry [10], and capillary electrophoresis [11], are renowned for their specificity and sensitivity. Despite their effectiveness, these conventional techniques are hampered by complex sample preparation processes, lengthy analysis time, and the necessity for sophisticated laboratory apparatus, making them less practical for rapid and on-site applications [12,13]. In pursuit of more efficient detection strategies, recent advancements have led to the development of innovative sensors leveraging colorimetry [14], chemiluminescence [15], surface-enhanced Raman spectroscopy [16],

* Corresponding author.
** Corresponding author.
*** Corresponding author.
E-mail addresses: mapinyi@jlu.edu.cn (P. Ma), gaodejiang@jlu.edu.cn (D. Gao), songdq@jlu.edu.cn (D. Song).

https://doi.org/10.1016/j.talanta.2024.126382
Received 3 April 2024; Received in revised form 28 May 2024; Accepted 5 June 2024
Available online 6 June 2024

electrochemiluminesce [17], and fluorometry [18]. Fluorometric methods, in particular, have garnered significant interest due to their exceptional sensitivity, straightforward operation, rapid response, and the convenience of visual detection [19]. Traditional fluorescent sensors, however, typically depend on the variation in a single fluorescence signal, rendering them vulnerable to environmental, instrumental, and background interferences [20]. To overcome these limitations, the advent of ratiometric fluorescent sensors, characterized by dual emission wavelengths, marks a significant leap forward. These sensors offer enhanced sensitivity and precision by minimizing external interferences through an inherent self-calibration mechanism [21,22]. Additionally, the vivid fluorescence color transitions inherent to ratiometric probes facilitate more intuitive visualization of target analytes [23].

Eu^{3+}-based fluorescence sensing platforms have attracted extensive attention from researchers owing to the unique optical characteristics of Eu^{3+}, such as narrow-band emission spectrum, bright red emission, large Stokes shift, and long fluorescence lifetime [24]. The β-diketone structure of OTC can coordinate with Eu^{3+} and transfer the absorbed energy to Eu^{3+}, thus sensitizing its characteristic fluorescence. This effect is known as the "antenna effect" [25,26]. The Eu^{3+}-OTC complex has weak emission and poor sensitivity during OTC detection due to the quenching effect caused by the high frequency vibrations of O–H bonds in water molecules chelated with Eu^{3+} [27]. Enhancing the fluorescence intensity and sensitivity by substituting these coordinated water molecules with auxiliary ligands represents a potential strategy [28,29]. However, the realization of ratiometric fluorescent detection for OTC poses considerable challenges, necessitating innovative approaches to address these limitations.

The rational selection of fluorescent nanomaterials plays a pivotal role in providing an additional fluorescence response for ratiometric detection. Molybdenum disulfide quantum dots (MoS_2 QDs) have many advantages including excellent optical properties, good water solubility, favorable biocompatibility, and low toxicity. These advantages can render MoS_2 QDs as an ideal candidate for biological imaging and fluorescence sensing [30,31]. Additionally, the hydrothermal method is an attractive approach for synthesizing MoS_2 QDs because of its high efficiency, facile operation, and environmental friendliness [32]. So far, some sensors based MoS_2 QDs have been developed for the analysis of OTC. For instance, Yu et al. [33] designed a single-emission fluorescent sensor for OTC detection based on the fluorescence quenching effect of OTC on MoS_2 QDs. More recently, Wu et al. [34] developed a ratiometric fluorescent OTC sensor by encapsulating MoS_2 QDs in ZIF-8. However, the single-emission sensor was susceptible to environmental interference and had a narrow liner detection range. As for the nanohybrid sensor, the synthesis process was cumbersome and time-consuming. To overcome these problems, a novel ratiometric fluorescence sensor for OTC detection was developed by simply mixing MoS_2 QDs with Eu^{3+}.

In this work, we developed a dual-response ratiometric fluorescent sensor through the self-assembly of blue-emissive MoS_2 QDs prepared by a facile hydrothermal method and Eu^{3+} for determination of OTC (Scheme 1). The sensor operates on a nuanced mechanism: the introduction of OTC leads to a reduction in the fluorescence intensity of MoS_2 QDs, a consequence of the inner filter effect (IFE) induced by OTC. Concurrently, the characteristic red fluorescence of Eu^{3+} experiences an upsurge, facilitated by the energy transfer from OTC to Eu^{3+} through the antenna effect (AE). This intricate interplay between the two fluorescence responses forms the basis of our ratiometric probe, characterized by its high sensitivity and selectivity towards OTC detection. The observable shift in fluorescence color from blue to red with increasing OTC concentrations, discernible even to the naked eye under a 365 nm ultraviolet lamp, underscores the sensor's practical utility. Additionally, the sensor's efficacy was validated through the detection of OTC in adulterated pure milk and mutton samples, highlighting its potential as a versatile tool in food safety analysis.

2. Experimental section

2.1. Synthesis of MoS_2 QDs

Water-soluble MoS_2 QDs were synthesized by hydrothermal method

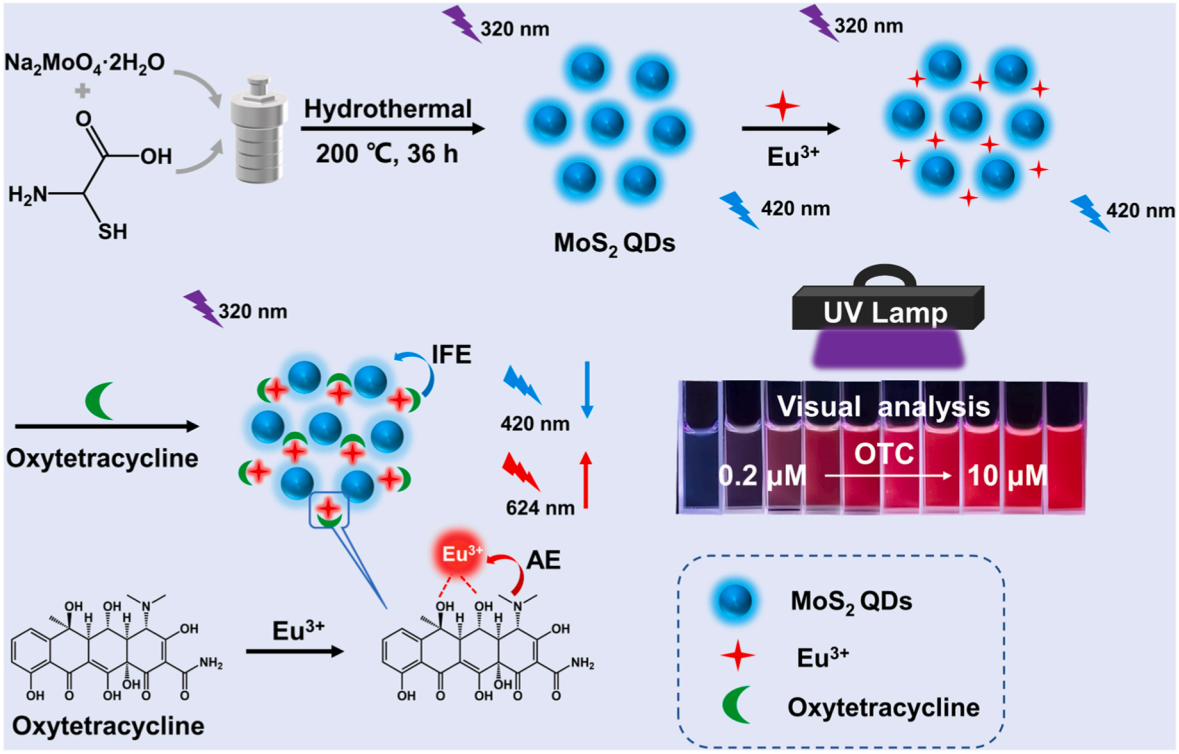

Scheme 1. Schematic illustration demonstrating the preparation of MoS_2 QDs and the principle for OTC detection of MoS_2 QDs/Eu^{3+}-based ratiometric fluorescent sensor.

according to a previous method with slight modifications [32]. Initially, 0.25 g of $Na_2MoO_4{\cdot}2H_2O$ was dissolved in 25 mL of deionized water and subjected to ultrasonication for 5 min to ensure complete dissolution. Then, the solution pH was adjusted to 6.5 using 0.1 M HCl. Following pH adjustment, 0.5 g of L-cysteine, along with an additional 50 mL of deionized water, was introduced to the solution. This mixture underwent a further 10 min of ultrasonication to achieve homogeneity. The resultant homogeneous mixture was then transferred to a 100 mL Teflon-lined stainless-steel autoclave, where it was subjected to a hydrothermal reaction at 200 °C for an extended duration of 36 h. Upon completion of the reaction and subsequent cooling to ambient temperature, the mixture was centrifuged at 12,000 rpm for 20 min to separate the supernatant containing the MoS_2 QDs. This supernatant was then meticulously filtered through a 0.22 μm microporous membrane to eliminate any particulate matter. To attain a higher purity of MoS_2 QDs, the filtered solution underwent dialysis against ultrapure water for 24 h, utilizing an MD44 dialysis bag with a molecular weight cut-off (MWCO) of 1000 Da. The purified MoS_2 QDs were subsequently stored at 4 °C, pending further experimental use.

2.2. Detection of oxytetracycline with MoS_2 QDs/Eu^{3+} sensor

The procedure for detecting oxytetracycline with the MoS_2 QDs/Eu^{3+} sensor commenced by preparing the sensing mixture. Specifically, 50 μL of MoS_2 QDs and 40 μL of 1 mM Eu^{3+} solution were combined with 500 μL of Tris-HCl buffer (10 mM, pH 7.0). To this mixture, oxytetracycline at varying concentrations (0.2–10 μM) was introduced, and the total volume was subsequently brought up to 1 mL with ultrapure water to ensure proper dilution. Following thorough mixing to ensure homogeneity, the reaction mixtures were allowed to incubate at ambient temperature for 80 s, facilitating the interaction between the sensor components and oxytetracycline. Post-incubation, the fluorescence emission spectra of the mixtures were meticulously recorded over a range from 340 nm to 700 nm, employing an excitation wavelength of 320 nm. The excitation and emission slit widths were set to 5 nm, and the photomultiplier voltage was adjusted to 700 V.

2.3. Selectivity and anti-interference experiments

To ascertain the selectivity of the developed OTC detection sensor, OTC was substituted with a variety of potential interfering substances in the testing protocol. These included a range of antibiotics such as tetracycline (TC), doxycycline (DOC), chlortetracycline (CTC), chloramphenicol (CAP), sulfadiazine (SD), vancomycin (VAN), penicillin G (Pen G), and sulfadimethoxine (SDM); essential amino acids like histidine (His), arginine (Arg), aspartic acid (Asp), and phenylalanine (Phe); and common inorganic ions including sodium (Na^+), potassium (K^+), calcium (Ca^{2+}), magnesium (Mg^{2+}), chloride (Cl^-), sulfate (SO_4^{2-}), and nitrate (NO_3^-). Furthermore, the sensor's resistance to interference was rigorously tested in a complex matrix containing both OTC and the aforementioned potential interferences, employing the identical methodology delineated in section 2.2.

2.4. Real sample analysis

The practical applicability of the sensor was validated using real food matrices, specifically pure milk and mutton. The milk was sourced from a local supermarket, while the mutton was procured from the Jilin Academy of Agricultural Sciences. The samples were processed according to previous methods with slight modifications [35,36].

For milk analysis, 2 mL of the sample was mixed with 4 mL of ethanol to facilitate the precipitation of proteins and lipids. This mixture was then subjected to ultrasonication for 15 min, followed by centrifugation at 5000 rpm for 10 min. The clear supernatant obtained was further centrifuged, then passed through a 0.22 μm membrane filter to remove any remaining particulate matter. The resultant filtrate was diluted with deionized water in preparation for analysis.

Mutton samples were processed by homogenizing 1 g of tissue with 3 mL of ethanol, followed by vortex mixing for 3 min and ultrasonication for 15 min. Post-centrifugation, the supernatant was filtered and similarly diluted with deionized water.

These prepared real samples were then spiked with OTC at varying concentrations (2.00, 5.00, and 8.00 μM) to assess the sensor's performance in complex biological matrices, utilizing the detection protocol outlined in section 2.2.

3. Results and discussion

3.1. Characterization of MoS_2 QDs

MoS_2 QDs could be easily synthesized via a hydrothermal method using sodium molybdate dihydrate as a molybdenum source and L-Cysteine as a sulfur source. As displayed in the TEM image, the prepared MoS_2 QDs were evenly distributed spherical nanoparticles with an average diameter of 2.84 nm (Fig. 1A&B). The parallel and clear lattice fringes of MoS_2 QDs can be observed in the high-resolution TEM image (Inset of Fig. 1A).

The FT-IR spectrum showed the surface functional groups of MoS_2 QDs (Fig. 1C). The weak peak at 462 cm^{-1} was due to the Mo–S vibration [32]. The broad absorption band at 3000–3600 cm^{-1} corresponded to the N–H/O–H stretching vibration. The absorption peaks observed at 2972 cm^{-1} and 2932 cm^{-1} corresponded to the asymmetric C–H stretching vibration. The characteristic peak at 1570 cm^{-1} corresponded to the in-plane stretching vibration of N–H. The peak at 1420 cm^{-1} can be ascribed to the symmetric stretching vibration of C═O. The peak corresponding to the stretching vibration of C–N was observed at 1300 cm^{-1} [37,38]. These results illustrate the presence of abundant carboxyl and amino groups on the surface of MoS_2 QDs. Therefore, the MoS_2 QDs have excellent water solubility and are convenient to be functionalized.

The XPS spectrums were measured to analyze the elemental composition and surface chemical state of the prepared MoS_2 QDs. In the full-scan survey (Fig. 1D), the diffraction peaks for Mo, S, C, N, O, and Na involved in hydrothermal synthesis were observed. Four single peaks were observed in the high-resolution spectra of S 2p (Fig. 1E). Two peaks at 163.37 and 164.59 eV were associated with the S $2p_{3/2}$ and S $2p_{1/2}$ orbitals of MoS_2. Other two peaks at 168.36 eV (S $2p_{3/2}$) and 169.59 eV (S $2p_{1/2}$) were likely derived from the $S_2O_3^{2-}$ group. The high-resolution Mo 3 d spectra exhibited main characteristic peaks at 225.95 eV, 227.75 eV, and 230.10 eV, which corresponded to the S 2s, Mo^{4+} $3d_{5/2}$ and Mo^{4+} $3d_{3/2}$ lines of MoS_2, respectively. The peak at 232.33 eV, which can be assigned to Mo^{6+} $3d_{3/2}$, was the result of Na_2MoO_4 residues or the slight oxidation of Mo^{4+} (Fig. 1F) [39,40]. All the above results confirm the successful preparation of MoS_2 QDs.

3.2. Optical properties of MoS_2 QDs

The optical characteristics of the MoS_2 QDs were thoroughly examined through UV–vis absorption spectroscopy and fluorescence spectroscopy. As shown in Fig. 2A, the UV–Vis absorption spectrum featured a notable shoulder absorption band at 270 nm, indicative of the excitonic properties inherent to MoS_2 QDs [41].

Furthermore, the MoS_2 QDs demonstrated a prominent fluorescence emission peak at 420 nm when excited at a wavelength of 320 nm (Fig. 2A). Under a 365 nm ultraviolet lamp, the solution of MoS_2 QDs exhibited a vivid blue fluorescence (Inset of Fig. 2A). The excitation-dependent emission behavior of MoS_2 QDs, spanning from 420 to 442 nm across excitation wavelengths of 280–360 nm, was characterized by a gradual increase in fluorescence intensity peaking at 320 nm, followed by a subsequent decrease (Fig. 2B). This behavior is attributed to the hot photoluminescence from the K point of the Brillouin zone and the polydispersity of the QDs [42].

Additionally, the fluorescence stability of MoS_2 QDs was assessed in

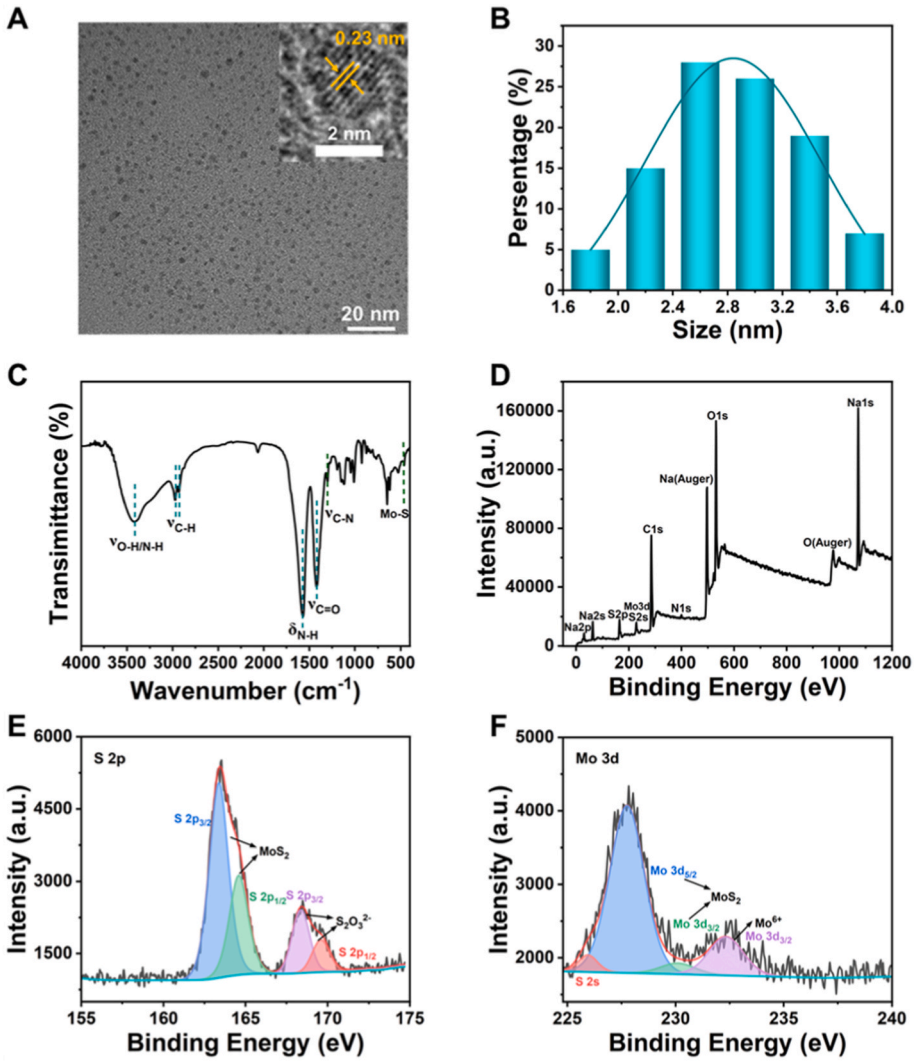

Fig. 1. (A) TEM image of MoS_2 QDs (Inset: the HR-TEM image of MoS_2 QDs). (B) Size distribution of MoS_2 QDs. (C) FT-IR spectrum of MoS_2 QDs. (D) XPS survey spectra of MoS_2 QDs. (E&F) High-resolution peak-fitting XPS spectra of (E) S 2p and (F) Mo 3 d orbitals.

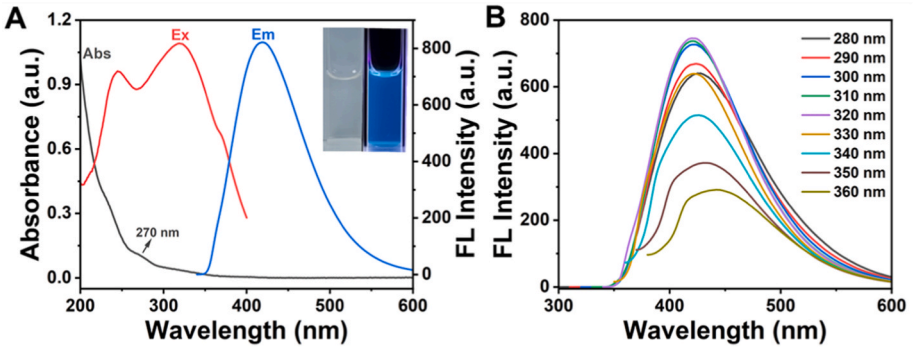

Fig. 2. (A) UV–vis absorption spectra, and fluorescence excitation and emission spectra of MoS_2 QDs (Inset: photographs of MoS_2 QDs under daylight (left) and ultraviolet light (right)). (B) Fluorescence emission spectra of MoS_2 QDs under different excitation wavelengths.

varying environmental conditions, including pH, ionic strength, temperature and ultraviolet light radiation time. The fluorescence intensity of the QDs remained largely consistent across a pH range of 3.0–10.0, indicating excellent pH stability (Fig. S1A). Moreover, the QDs displayed remarkable tolerance to high ionic strength, maintaining stable fluorescence even in 100 mM NaCl solutions (Fig. S1B). As shown in Fig. S1C, the fluorescence intensity of the QDs decreased slightly with the increase of temperature, but remained relatively stable even when the system temperature reached 95 °C. The fluorescence intensity of the QDs showed little change under contious exposure to ultraviolet light for 55 min, demonstrating their good photostability (Fig. S1D). These results indicate that the developed MoS_2 QDs possess excellent fluorescence stability and are therefore suitable for further analysis and detection applications.

3.3. Sensor material selection and sensing mechanism

MoS_2 QDs and Eu^{3+} were selected as materials for constructing a dual-response ratiometric fluorescent OTC detection probe due to the following reasons. First, the excitation and emission spectra of MoS_2 QDs largely overlapped with the absorption spectrum of OTC. This allows OTC to effectively quench the fluorescence of MoS_2 QDs through the internal filtering effect (IFE) or fluorescence resonance energy transfer (FRET) (Fig. 3A) [43]. Second, OTC has a β-diketone structure and a high molar extinction coefficient; thus, it can chelate with Eu^{3+} and transfer energy to Eu^{3+}, thereby allowing for the sensitization of the Eu^{3+} luminescence through the antenna effect [19]. Additionally, the emission peak of MoS_2 QDs at 420 nm was largely shifted in contrast with the characteristic peak of Eu^{3+} at 624 nm originated from the $^5D_0 \rightarrow {}^7F_2$ transition, which can greatly avoid the spectral overlap of different emission peaks. For the above reasons, MoS_2 QDs and Eu^{3+} can be used as the identification units for OTC to achieve opposite variation of two fluorescence signals, which is convenient for developing a ratiometric fluorescent sensor.

To verify that the MoS_2 QDs/Eu^{3+}-based ratiometric fluorescent probe can determine OTC, relevant experiments were conducted. The Zeta potentials were performed to characterize the state of Eu^{3+} on the surface of MoS_2 QDs. As shown in Fig. S2, the MoS_2 QDs were negatively charged, which may due to the abundant carboxyl on the surface of MoS_2 QDs. After mixing with Eu^{3+}, the zeta potential of MoS_2 QDs-Eu^{3+} was measured to be +6.71 mV, indicating the electrostatic interaction between MoS_2 QDs and Eu^{3+}. It was noted in Fig. 3B that the introduction of Eu^{3+} had negligible influence on the fluorescence intensity of MoS_2 QDs, and the characteristic fluorescence of Eu^{3+} could not be sensitized by MoS_2 QDs (black and red curves). When OTC was introduced into the MoS_2 QDs/Eu^{3+} system, the fluorescence intensity of MoS_2 QDs at 420 nm decreased, while that of Eu^{3+} at 624 nm obviously increased (blue curve). Therefore, it is clear that the dual-response MoS_2 QDs/Eu^{3+} ratiometric fluorescent sensor for OTC detection was successfully developed.

We carried out a series of experiments to illustrate the sensing mechanism of the MoS_2 QDs/Eu^{3+} ratiometric fluorescent sensor during the detection of OTC. First, related time-resolved fluorescence decay tests were performed to investigate the mechanism of OTC in inducing the fluorescence quenching of MoS_2 QDs. While FRET can lead to the shortening of the fluorescence lifetime of fluorophores, IFE cannot [43]. Fig. 3C shows that the fluorescence lifetimes of MoS_2 QDs, MoS_2 QDs-Eu^{3+} and MoS_2 QDs -Eu^{3+}-OTC at 420 nm were 6.47, 6.57, and 6.52 ns, respectively. The fluorescence lifetime of MoS_2 QDs remained unchanged despite the introduction of OTC, which suggests that the fluorescence quenching of MoS_2 QDs is mainly due to IFE.

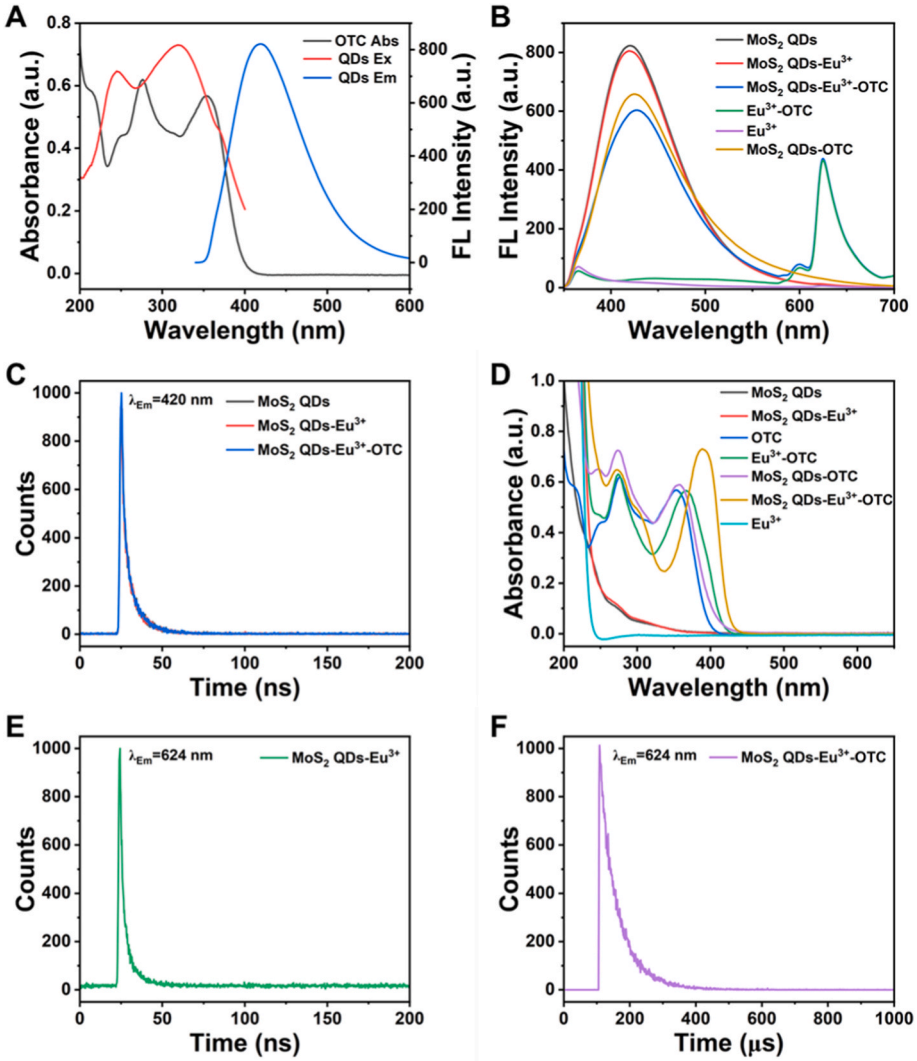

Fig. 3. (A) UV–vis absorption spectra of OTC, and fluorescence excitation and emission spectra of MoS_2 QDs. (B) Feasibility in using the proposed sensor for OTC detection: fluorescence spectra of different systems. (C) Decay curves of fluorescence at 420 nm of MoS_2 QDs, MoS_2 QDs-Eu^{3+} and MoS_2 QDs-Eu^{3+}-OTC. (D) UV–vis absorption spectra of different systems. (E&F) Decay curves of fluorescence at 624 nm of (E) MoS_2 QDs-Eu^{3+} and (F) MoS_2 QDs-Eu^{3+}-OTC.

Furthermore, the mechanism of Eu^{3+} fluorescence enhancement was investigated. As shown in Fig. 3D, the main absorption peak of OTC in MoS_2 QDs-Eu^{3+}-OTC system was red-shifted from 353 to 390 nm, and the absorption intensity also enhanced greatly (yellow curve). Morever, the main absorption peak of OTC was not obviously shifted in MoS_2 QDs-OTC system (purple curve). These observations suggest that OTC was successfully chelated with Eu^{3+}. Fig. 3E and F illustrate that the fluorescence lifetime of Eu^{3+} at 624 nm increased significantly from 5.14 ns to 57.77 μs upon the addition of OTC, which further demonstrates that OTC can transfer energy to Eu^{3+} and sensitize its luminescence through the antenna effect.

3.4. Optimization of assay conditions

To optimize the analytical performance of the sensor in OTC detection, several reaction variables including Eu^{3+} concentration, solution pH, and reaction time were investigated. The performance of the sensor at different Eu^{3+} concentrations was investigated. As depicted in Fig. S3A, the fluorescence intensity ratio (F_{624}/F_{420} ratio) gradually increased with the increase of Eu^{3+} concentration and was stable when Eu^{3+} concentration reached 40 μM. Thus, 40 μM Eu^{3+} was used in subsequent experiments. The influence of pH ranging from pH 4.0 to pH 10.0 on the sensing system was further studied. As displayed in Fig. S3B, the F_{624}/F_{420} ratio reached a maximum value at pH 7.0. Thus, pH 7.0 was selected as the optimal pH and employed in the following tests. The F_{624}/F_{420} ratio increased rapidly within the first 80 s and was nearly unchanged thereafter. This suggests that the optimal reaction time is 80 s (Fig. S3C). Overall, Eu^{3+} at a concentration of 40 μM, pH 7.0, and an equilibration time of 80 s were considered the optimal experimental conditions and applied in the subsequent study.

3.5. Fluorescence sensing of oxytetracycline via MoS_2 QDs/Eu^{3+}-based ratiometric fluorescent sensor

The performance of the MoS_2 QDs/Eu^{3+}-based ratiometric fluorescent probe in quantitatively detecting OTC was assessed under the optimal conditions. As displayed in Fig. 4A, with increasing OTC concentration, the fluorescence intensity at 420 nm gradually decreased, while that at 624 nm increased. Good linear relationship between the F_{624}/F_{420} ratio and OTC concentration ranging from 0.2 to 10 μM was observed, and the regression equation was $F_{624}/F_{420} = 0.07711[OTC] + 0.01563$ ($R^2 = 0.9987$) (Fig. 4B). The detection limit (LOD) was calculated to be 2.21 nM based on equation 3δ/S (where δ is the standard deviation of blank samples (n = 9) and S is the slope of the calibration curve). Moreover, as the OTC concentration was increased, the fluorescence color of the sensing system gradually changed from blue to red under the illumination of a 365 nm ultraviolet lamp (Inset of Fig. 4A). This color variation was also visible to the naked eye. The above observations show that the proposed method can be employed as a visual sensor for semi-quantitative detection of OTC.

The comparison between this sensing strategy and other OTC detection methods is listed in Table S1. The comparison showed that most methods had complex material preparation process and long detection time. The proposed sensor had a wider linear range, a lower detection limit and shorter detection time than most of other methods. Furthermore, our detection limit was well below the maximum residue limits set by the World Health Organization (220 nM). Therefore, our method was more convenient, suitable and time saving for OTC determination in practical application.

3.6. Selectivity and anti-interference of MoS_2 QDs/Eu^{3+}-based ratiometric sensor

To assess the selectivity to OTC of the MoS_2 QDs/Eu^{3+}-based ratiometric probe, the fluorescence response of the sensor to potential interferences, including common antibiotics (10 μM), amino acids, and inorganic ions (100 μM), was studied. As shown in Fig. 5A, only tetracycline antibiotics (including TC, DOC, and CTC) caused obvious changes in the F_{624}/F_{420} ratio, while other interferences showed negligible influence, and this could be attributed to their similar structures and functional groups to OTC (Fig. S4). Among the four antibiotics, OTC had the strongest response to the sensor, which could be due to its higher number of hydroxyl substituent groups, resulting in higher charge density and stronger binding affinity to Eu^{3+}. In this work, OTC was selected as a representative for specific analysis. The anti-interference analysis was performed in the presence of both OTC and possible interferences. As displayed in Fig. 5B, the difference in the F_{624}/F_{420} ratio between other interferences coexisting with OTC and OTC alone was not obvious. These results verify that the proposed sensor exhibits good selectivity to OTC and anti-interference ability.

3.7. Application in real samples

The efficacy of the proposed sensor for OTC detection was rigorously evaluated in complex matrices, specifically pure milk and mutton samples, employing the standard addition method. The results, summarized in Table 1, demonstrate notable accuracy in OTC quantification within these food matrices, with recovery rates ranging from 100.3 % to 116.9 % for milk and 99.4 %–109.4 % for mutton. Moreover, the observed relative standard deviation (RSD) values were consistently below 3 %, underscoring the sensor's reliability and precision. These findings substantiate the sensor's potential as an effective tool for OTC determination in food samples, highlighting its suitability for practical applications in ensuring food safety.

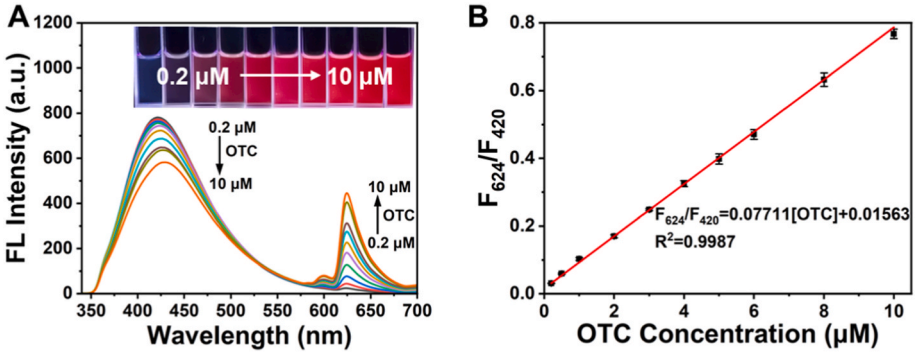

Fig. 4. (A) Fluorescence emission spectra of MoS_2 QDs/Eu^{3+} in the presence of OTC at different concentrations (Inset: the corresponding fluorescent photographs taken under a 365 nm ultraviolet lamp, the concentrations of OTC from left to right in the upper image were 0.2, 0.5, 1, 2, 3, 4, 5, 6, 8, and 10 μM). (B) Linear relationship between F_{624}/F_{420} and OTC concentration.

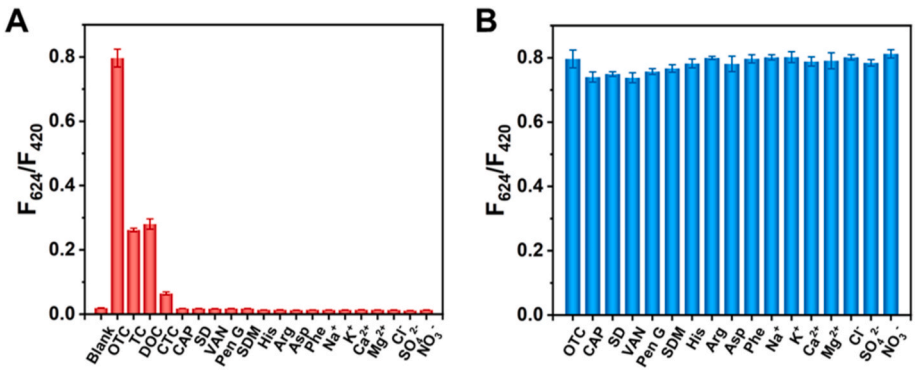

Fig. 5. (A) Selectivity to OTC and (B) anti-interference properties of the proposed sensor evaluated in the presence of various antibiotics (10 μM), amino acids, and inorganic ions (100 μM).

Table 1
Determination of OTC in actual and spiked samples (n = 3).

Samples	Spiked (μM)	Found (μM)	Recovery (%)	RSD (%)
Milk	2.00	2.34 ± 0.015	116.9	0.65
	5.00	5.14 ± 0.072	102.7	1.40
	8.00	8.03 ± 0.121	100.3	1.50
Mutton	2.00	2.19 ± 0.007	109.4	0.30
	5.00	5.03 ± 0.123	106.2	2.45
	8.00	7.96 ± 0.153	99.4	1.92

4. Conclusions

In summary, we constructed a dual-response ratiometric fluorescent OTC detection platform based on MoS_2 QDs/Eu^{3+}. The introduction of OTC could weaken the blue fluorescence of MoS_2 QDs due to the inner filter effect, while the characteristic red emission of Eu^{3+} was enhanced due to the energy transfer from OTC to Eu^{3+} via the antenna effect. The developed sensor had a linear response at OTC concentration ranging from 0.2 to 10 μM and a low LOD of 2.21 nM. The fluorescence response of the sensor to OTC could be completed within 80 s, which is considered rapid. Furthermore, the fluorescent color of the sensing system changed from blue to red, making a potential tool for the visual assay of OTC. With its high selectivity and sensitivity towards OTC, the sensor was successfully applied to detect OTC in spiked pure milk and mutton samples with satisfactory recoveries. Overall, the developed sensor is a promising tool for rapid detection of OTC residues in food samples.

CRediT authorship contribution statement

Mengjia Guo: Writing – original draft, Methodology, Investigation, Formal analysis, Conceptualization. **Ming Bi:** Validation, Investigation, Data curation. **Fangmei Zhang:** Visualization, Validation, Resources, Data curation. **Xiwen Ye:** Software, Investigation, Formal analysis, Data curation. **Pinyi Ma:** Writing – review & editing, Supervision, Project administration. **Dejiang Gao:** Writing – review & editing, Supervision, Funding acquisition. **Daqian Song:** Project administration, Funding acquisition.

Declaration of competing interest

The authors declare that they have no known competing financial interests or personal relationships that could have appeared to influence the work reported in this paper.

Data availability

Data will be made available on request.

Acknowledgments

This work was supported by the National Key R&D Program of China (2022YFF0710404), and the Science and Technology Developing Foundation of Jilin Province of China (Nos. 20210101262JC, 20230101033JC, and 20230204116YY).

Appendix A. Supplementary data

Supplementary data to this article can be found online at https://doi.org/10.1016/j.talanta.2024.126382.

References

[1] C.-H. Kim, L.-P. Lee, J.-R. Min, M.-W. Lim, S.-H. Jeong, An indirect competitive assay-based aptasensor for detection of oxytetracycline in milk, Biosens. Bioelectron. 51 (2014) 426–430.
[2] P. Su, L. Yu, Y. Ai, S. Zhang, H. Ge, Y. Bu, D. Huang, X. Wang, S. Wang, Conformational fixation induced fluorescence turn-on of oxytetracycline coordinated on aluminum-based metal-organic frameworks for ultrasensitive sensing application, Sensor. Actuator. B Chem. 368 (2022) 132043.
[3] C. Cháfer-Pericás, Á. Maquieira, R. Puchades, J. Miralles, A. Moreno, Multiresidue determination of antibiotics in feed and fish samples for food safety evaluation. Comparison of immunoassay vs LC-MS-MS, Food Control 22 (6) (2011) 993–999.
[4] H. Zhang, R. Li, Z. Li, Excitation-depended fluorescence emission of boron-doped graphene quantum dot as an optical probe for detection of oxytetracycline in food and information encryption patterns, Microchim. Acta 190 (7) (2023) 278.
[5] N. Zhou, Y. Ma, B. Hu, L. He, S. Wang, Z. Zhang, S. Lu, Construction of Ce-MOF@COF hybrid nanostructure: Label-free aptasensor for the ultrasensitive detection of oxytetracycline residues in aqueous solution environments, Biosens. Bioelectron. 127 (2019) 92–100.
[6] C. Li, L. Zhu, W. Yang, X. He, S. Zhao, X. Zhang, W. Tang, J. Wang, T. Yue, Z. Li, Amino-functionalized Al-MOF for fluorescent detection of tetracyclines in milk, J. Agric. Food Chem. 67 (4) (2019) 1277–1283.
[7] K. Yan, Y. Liu, Y. Yang, J. Zhang, A cathodic "signal-off" photoelectrochemical aptasensor for ultrasensitive and selective detection of oxytetracycline, Anal. Chem. 87 (24) (2015) 12215–12220.
[8] Y. Wang, P. Ni, S. Jiang, W. Lu, Z. Li, H. Liu, J. Lin, Y. Sun, Z. Li, Highly sensitive fluorometric determination of oxytetracycline based on carbon dots and Fe_3O_4 MNPs, Sensor. Actuator. B Chem. 254 (2018) 1118–1124.
[9] J. Han, D. Jiang, T. Chen, W. Jin, Z. Wu, F. Cui, Simultaneous determination of olaquindox, oxytetracycline and chlorotetracycline in feeds by high performance liquid chromatography with ultraviolet and fluorescence detection adopting online synchronous derivation and separation, J. Chromatogr. B 1152 (2020) 122253.
[10] A. Gajda, A. Jablonski, T. Bladek, A. Posyniak, Oral fluid as a biological material for antemortem detection of oxytetracycline in pigs by liquid chromatography-tandem mass spectrometry, J. Agric. Food Chem. 65 (2) (2017) 494–500.
[11] T.A. Ferreira, J.F. Flores-Aguilar, E.M. Santos, J.A. Rodriguez, I.S. Ibarra, New poly (ionic liquid) based fiber for determination of oxytetracycline in milk samples by application of SPME-CE technique, Molecules 24 (3) (2019) 430.
[12] K. Birader, P. Kumar, Y. Tammineni, J.A. Barla, S. Reddy, P. Suman, Colorimetric aptasensor for on-site detection of oxytetracycline antibiotic in milk, Food Chem. 356 (2021) 129659.
[13] Z. Yang, X. Yang, Y. Zhang, X. Fan, Y. Cao, Z. Li, C. Dong, Detection of oxytetracycline in milk using a novel carbon dots-based fluorescence probe via facile pyrolysis synthesis, Environ. Sci. Pollut. Res. 30 (35) (2023) 84002–84010.
[14] Z. Chen, Y. Wang, Y. Mo, X. Long, H. Zhao, L. Su, Z. Duan, Y. Xiong, ZIF-8 directed templating synthesis of CeO_2 nanoparticles and its oxidase-like activity for colorimetric detection, Sensor. Actuator. B Chem. 323 (2020) 128625.

[15] M. Amjadi, T. Hallaj, F. Mirbirang, A chemiluminescence reaction consisting of manganese(IV), sodium sulfite, and sulfur- and nitrogen-doped carbon quantum dots, and its application for the determination of oxytetracycline, Microchim. Acta 187 (3) (2020) 191.
[16] K.-M. Lee, D. Yarbrough, M.M. Kozman, T.J. Herrman, J. Park, R. Wang, D. Kurouski, Rapid detection and prediction of chlortetracycline and oxytetracycline in animal feed using surface-enhanced Raman spectroscopy (SERS), Food Control 114 (2020) 107243.
[17] M. Ding, S. Zhang, J. Wang, Y. Ding, C. Ding, Ultrasensitive ratiometric electrochemiluminescence sensor with an efficient antifouling and antibacterial interface of PSBMA@SiO_2-MXene for oxytetracycline trace detection in the marine environment, Anal. Chem. 95 (44) (2023) 16327–16334.
[18] Y. Yang, X. Liu, S. Meng, S. Mao, W. Tao, Z. Li, Molecularly imprinted polymers-isolated AuNP-enhanced CdTe QD fluorescence sensor for selective and sensitive oxytetracycline detection in real water samples, J. Hazard Mater. 458 (2023) 131941.
[19] L. Han, Y.Z. Fan, M. Qing, S.G. Liu, Y.Z. Yang, N.B. Li, H.Q. Luo, Smartphones and test paper-assisted ratiometric fluorescent sensors for semi-quantitative and visual assay of tetracycline based on the target-induced synergistic effect of antenna effect and inner filter effect, ACS Appl. Mater. Interfaces 12 (41) (2020) 47099–47107.
[20] X. Hu, Y. Guo, J. Zhang, X. Wang, G. Fang, S. Wang, A signal-amplified ratiometric fluorescence biomimetic sensor based on the synergistic effect of IFE and AE for the visual smart monitoring of oxytetracycline, Chem. Eng. J. 433 (2022) 134499.
[21] X. Mu, X. Jiang, Y. Zhang, X. Liu, S. Zhang, W. Wang, Y. Huang, P. Ma, D. Song, Sensitive ratiometric fluorescence probe based on chitosan carbon dots and calcein for Alkaline phosphatase detection and bioimaging in cancer cells, Anal. Chim. Acta 1188 (2021) 339163.
[22] P. Sun, D. Yang, J. Li, Y. Zhang, Aggregation-induced emission of 4-formyl-3-hydroxybenzoic acid for the ratiometric fluorescence detection of tetracycline antibiotics, Dyes, Pigments 197 (2022) 109841.
[23] A. Bigdeli, F. Ghasemi, S. Abbasi-Moayed, M. Shahrajabian, N. Fahimi-Kashani, S. Jafarinejad, M.A. Farahmand Nejad, M.R. Hormozi-Nezhad, Ratiometric fluorescent nanoprobes for visual detection: design principles and recent advances-A review, Anal. Chim. Acta 1079 (2019) 30–58.
[24] H. Wei, Z. Zhao, C. Wei, G. Yu, Z. Liu, B. Zhang, J. Bian, Z. Bian, C. Huang, Antiphotobleaching: a type of structurally rigid chromophore ready for constructing highly luminescent and highly photostable europium complexes, Adv. Funct. Mater. 26 (13) (2016) 2085–2096.
[25] K. Yang, P. Jia, J. Hou, T. Bu, X. Sun, Y. Liu, L. Wang, Innovative dual-emitting ratiometric fluorescence sensor for tetracyclines detection based on boron nitride quantum dots and europium ions, ACS Sustain. Chem. Eng. 8 (46) (2020) 17185–17193.
[26] H.-Q. Yin, X.-Y. Wang, X.-B. Yin, Rotation restricted emission and antenna effect in single metal-organic frameworks, J. Am. Chem. Soc. 141 (38) (2019) 15166–15173.
[27] Y.J. Fan, Z.G. Wang, M. Su, X.T. Liu, S.G. Shen, J.X. Dong, A dual-signal fluorescent colorimetric tetracyclines sensor based on multicolor carbon dots as probes and smartphone-assisted visual assay, Anal. Chim. Acta 1247 (2023) 340843.
[28] F. Hijaz, Y. Nehela, O. Batuman, N. Killiny, Citrate mediated europium-based detection of oxytetracycline in citrus tissues, Antibiotics 10 (5) (2021) 566.
[29] E.F.C. Simões, J.M.M. Leitão, J.C.G. Esteves da Silva, NO fluorescence sensing by europium tetracyclines complexes in the presence of H_2O_2, J. Fluoresc. 23 (4) (2013) 681–688.
[30] Y. Yi, W. Zeng, G. Zhu, β-Cyclodextrin functionalized molybdenum disulfide quantum dots as nanoprobe for sensitive fluorescent detection of parathion-methyl, Talanta 222 (2021) 121703.
[31] X. Tang, X. Zeng, H. Liu, Y. Yang, H. Zhou, H. Cai, A nanohybrid composed of MoS_2 quantum dots and MnO_2 nanosheets with dual-emission and peroxidase mimicking properties for use in ratiometric fluorometric detection and cellular imaging of glutathione, Microchim. Acta 186 (8) (2019) 572.
[32] Y. Wang, Y. Ni, Molybdenum disulfide quantum dots as a photoluminescence sensing platform for 2,4,6-trinitrophenol detection, Anal. Chem. 86 (15) (2014) 7463–7470.
[33] X. Yu, Y. Meng, Y. Yan, X. Jin, G. Ni, J. Peng, Ethylenediamine functionalized MoS_2 quantum dots for terramycin sensing in environmental water and fish samples, Microchem. J. 152 (2020) 104406.
[34] J. Wu, X. Chang, Y. Guo, N. Xia, Synthesis of a hybrid nanocomposite: incorporating MoS_2 within a ZIF-8 for fluorescence-based detection and adsorption of tetracyclines antibiotics, Dyes, Pigments 226 (2024) 112137.
[35] M. Naseri, A. Niazi, K. Bagherzadeh, E. Konoz, H.R. Samadikhah, Modified electrochemical aptasensor for ultrasensitive detection of tetracycline: in silico and in vitro studies, Food Chem. 421 (2023) 136195.
[36] Q. Yang, H. Hong, Y. Luo, Heterogeneous nucleation and synthesis of carbon dots hybrid Zr-based MOFs for simultaneous recognition and effective removal of tetracycline, Chem. Eng. J. 392 (2020) 123680.
[37] X. Wang, J. Hou, S. Lan, C. Shen, D. Huo, Z. Ji, Y. Ma, H. Luo, S. Zhang, Q. He, C. Hou, MoS_2 QDs-Based sensor for measurement of fluazinam with triple signal output, Anal. Chim. Acta 1108 (2020) 152–159.
[38] L. Xie, Y. Yang, G. Gong, S. Feng, D. Liu, One-step hydrothermal synthesis of highly fluorescent MoS_2 quantum dots for lead ion detection in Aqueous Solutions, Nanomaterials 12 (19) (2022) 3329.
[39] Y. Zhong, L. Guo, Y. Zou, J. Ge, Y. Chen, Z. Lu, D. Wang, Cys-functionalized MoS_2 quantum dots and calcium ion for ratiometric fluorescence probes for doxycycline, ACS Appl. Nano Mater. 6 (23) (2023) 22355–22362.
[40] Y. Peng, W. Dong, L. Wan, X. Quan, Determination of folic acid via its quenching effect on the fluorescence of MoS_2 quantum dots, Microchim. Acta 186 (9) (2019) 605.
[41] M. Rong, J. Ye, B. Chen, Y. Wen, X. Deng, Z.-Q. Liu, Ratiometric fluorescence detection of stringent ppGpp using Eu-MoS_2 QDs test paper, Sensor. Actuator. B Chem. 309 (2020) 127807.
[42] W. Gu, Y. Yan, C. Zhang, C. Ding, Y. Xian, One-step synthesis of water-soluble MoS_2 quantum dots via a hydrothermal method as a fluorescent probe for hyaluronidase detection, ACS Appl. Mater. Interfaces 8 (18) (2016) 11272–11279.
[43] X. Mu, M. Wu, B. Zhang, X. Liu, S. Xu, Y. Huang, X. Wang, D. Song, P. Ma, Y. Sun, A sensitive “off-on” carbon dots-Ag nanoparticles fluorescent probe for cysteamine detection via the inner filter effect, Talanta 221 (2021) 121463.